Neural Networks 143 (2021) 148–160

Contents lists available at ScienceDirect

Neural Networks

journal homepage: www.elsevier.com/locate/neunet

Periodic clustering of simple and complex cells in visual cortex

Gwangsu Kim [a], Jaeson Jang [b], Se-Bum Paik [b,c,*]

[a] Department of Physics, Korea Advanced Institute of Science and Technology, Daejeon 34141, Republic of Korea
[b] Department of Bio and Brain Engineering, Korea Advanced Institute of Science and Technology, Daejeon 34141, Republic of Korea
[c] Program of Brain and Cognitive Engineering, Korea Advanced Institute of Science and Technology, Daejeon 34141, Republic of Korea

ARTICLE INFO

Article history:
Received 6 July 2020
Received in revised form 31 May 2021
Accepted 1 June 2021
Available online 5 June 2021

Keywords:
Primary visual cortex
Simple cell
Complex cell
Orientation map
Retinal mosaic
Feedforward projection

ABSTRACT

Neurons in the primary visual cortex (V1) are often classified as simple or complex cells, but it is debated whether they are discrete hierarchical classes of neurons or if they represent a continuum of variation within a single class of cells. Herein, we show that simple and complex cells may arise commonly from the feedforward projections from the retina. From analysis of the cortical receptive fields in cats, we show evidence that simple and complex cells originate from the periodic variation of ON–OFF segregation in the feedforward projection of retinal mosaics, by which they organize into periodic clusters in V1. From data in cats, we observed that clusters of simple and complex receptive fields correlate topographically with orientation maps, which supports our model prediction. Our results suggest that simple and complex cells are not two distinct neural populations but arise from common retinal afferents, simultaneous with orientation tuning.

1. Introduction

Neurons in the primary visual cortex (V1) are often classified as simple or complex cells (Hubel & Wiesel, 1962) by their characteristic organization of spatial receptive fields and the temporal dynamics of their response to stimuli. In traditional classifications, simple cells have segregated ON/OFF sub-regions of receptive fields and generate highly modulated sinusoidal response ($F_1/F_0 > 1$) to drifting gratings stimuli, while complex cells have largely overlapping ON/OFF sub-regions and generate weak modulation of response ($F_1/F_0 < 1$, Fig. 1a) (De Valois et al., 1982; Dean & Tolhurst, 1983; DeAngelis et al., 1995; Mata & Ringach, 2005; Nowak et al., 2010; Skottun et al., 1991). As suggested in the pioneering study of Hubel and Wiesel, simple and complex cells have often been considered to imply a hierarchically distinct functional architecture for visual processing (Antolik & Bednar, 2011; Lehky et al., 2005; Martinez & Alonso, 2003; Martinez et al., 2005), so that simple cells pool feedforward inputs (Ferster & Lindström, 1983; Reid & Alonso, 1995), while complex cells then pool inputs from the simple cells (Fig. 1b) (Alonso & Martinez, 1998; Yu & Ferster, 2013).

However, subsequent studies have raised the possibility that simple and complex neurons are not clearly distinct populations but might be variations within a continuous spectrum (Chance et al., 1999; Crowder et al., 2007; Fournier et al., 2011; Mechler & Ringach, 2002; Priebe et al., 2004; Tao et al., 2004). Although the conventional hierarchical model predicts that neurons in the early layer are mostly simple cells (Antolik & Bednar, 2011; Hubel & Wiesel, 1962) (Fig. 1c, top), it was reported that complex cells coexist with simple cells in layer 4 of monkey, which receives the majority of feedforward afferents from the thalamus (Fig. 1c, bottom Ringach et al., 2002). Similarly, in layer 4 of cat, most cells were classified as simple ones, but a significant portion of complex cells were also observed (Martinez et al., 2005). Thus, these results raise questions of the origin of simple and complex cells: Simple and complex cells are not clearly distinct populations, and may arise from non-distinctive neural circuits. If so, then what possible mechanism is there for the development of such a functional variation?

Recent studies have suggested that ON/OFF feedforward afferents play a crucial role in initiating diverse functional tuning of neurons in V1. The orientation preference of a cortical column can be predicted by the local arrangement of ON/OFF afferents (Jin et al., 2011; Lee et al., 2016) and other functional tuning such as direction selectivity (Lien & Scanziani, 2018), ON/OFF polarity, and ocular dominance (Kremkow et al., 2016) are observed to develop from the integration of thalamic feedforward inputs. Considering that an LGN neuron is modulated by only a small number of retinal ganglion cells (RGCs) in monkeys, cats, and mice (Litvina & Chen, 2017; Schein & de Monasterio, 1987; Usrey et al., 1999), and that local thalamic receptive fields preserve those of RGCs, the spatial distribution of ON/OFF retinal mosaics may induce the initial formation of functional tuning and their topographic organization in V1 (Ringach, 2004, 2007; Soodak, 1987).

* Corresponding author at: Program of Brain and Cognitive Engineering, Korea Advanced Institute of Science and Technology, Daejeon 34141, Republic of Korea.
E-mail address: sbpaik@kaist.ac.kr (S.-B. Paik).

https://doi.org/10.1016/j.neunet.2021.06.002

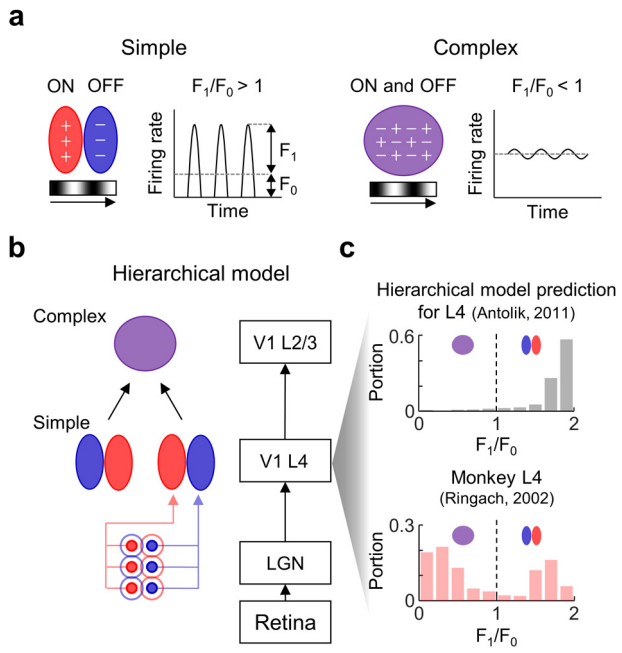

Fig. 1. Development of simple and complex cells in the primary visual cortex. (a) Illustration of simple (left) and complex (right) cells. Receptive fields and response profiles to a drifting sinusoidal grating stimulus are described. Red area (+): ON subregion. Blue area (−): OFF subregion. Purple area (+&−): both ON and OFF subregion. F_1/F_0: ratio of 1st harmonic amplitude to mean elevation of firing rate. (b) Schematic of the classical hierarchical model. (c) Bimodal histograms of F_1/F_0 in Layer 4 of adult monkeys (red bar, adapted from Fig. 11 of reference Ringach et al., 2002) and prediction of hierarchical model (gray bar, adapted from reference Antolik & Bednar, 2011). (For interpretation of the references to color in this figure legend, the reader is referred to the web version of this article.)

Here, we propose that the simple and complex tuning of V1 neurons arises from a common retinal mosaics structure, topographically correlated with the preferred orientation of underlying neurons. From the analysis of data in cats and monkeys, we show evidence that neuronal variation from simple to complex cells can be predicted from the segregation between local ON and OFF feedforward projections from the retina. We show that clusters of simple and complex receptive fields are observed across V1, the spatial period of which is similar to that of underlying orientation maps. Overall, our findings suggest that structured inputs from the retina can initiate simple-to-complex variations of the neural responses in V1, enabling a periodic organization of the simple and complex tuning in V1.

2. Results

2.1. Simple and complex cells from the spatial arrangement of ON/OFF retinal afferents

Based on the theory that functional tuning in the visual cortex originates from the afferent of ON and OFF RGC mosaics (Paik & Ringach, 2011, 2012; Ringach, 2004, 2007; Soodak, 1987) (Fig. 2a), we hypothesized that both simple and complex cells in V1 are initially seeded by the local projection of feedforward afferents and that the variation of the cell types depends on the spatial distribution of the ON and OFF receptive fields imprinted in the RGC mosaics (Fig. 2b). We introduced our model idea by investigating the profile of retinal mosaics data of ON-center and OFF-center receptive fields (RFs, Fig. 2c) (Gauthier et al., 2009). As previously reported (Gauthier et al., 2009; Wassle et al., 1981), the nearest neighbor distance between different types of RF centers ($d_{ON\text{-}OFF}$) appeared smaller than that between the same type (average of d_{ON-ON} = 116 μm and $d_{OFF\text{-}OFF}$ = 106 μm), thus the nearest neighbor of an ON cell appears to be an OFF cell, and vice versa. The profile of this ON–OFF distance ($d_{ON\text{-}OFF}$) measured from RGC mosaics data (Gauthier et al., 2009) showed a wide variation, well fitted to a Gaussian distribution (mean = 56.4 μm, standard deviation = 14.3 μm, R^2 = 0.91) (Fig. 2c, bottom histogram).

Our main hypothesis is that this spatial organization of ON and OFF RGCs can constrain the tuning of the connected V1 neurons as either simple or complex cells, via statistical wiring from the retina to V1 (Paik & Ringach, 2011, 2012; Ringach, 2004, 2007; Soodak, 1987). When the distance between ON and OFF RGC is large (Fig. 2d, green circle, $d_{ON\text{-}OFF}$ = 87 μm, top 12%), a V1 neuron that receives retinal afferents from these local ON and OFF RGCs has a receptive field of weakly overlapping ON and OFF sub-regions. This results in a high simpleness index (SI, 0.42, see Methods), representing simple cell-like segregation between ON/OFF subregions. In contrast, when the distance between ON and OFF RGCs is small (Fig. 2d, purple circle, $d_{ON\text{-}OFF}$ = 23 μm, bottom 5%), the inputs to V1 generate the receptive field of highly overlapping ON and OFF sub-regions with low SI (0.15), like a complex cell. In this scenario, the simple/complex tuning in V1 is strongly biased by variation of the local arrangement of ON and OFF RGC mosaics.

We show that the coexistence of simple and complex cells in layer 4 of monkeys can be initiated from the structure of measured RGC mosaics, from variation of the response modulated by the distance between ON and OFF subregions of RF. We considered F_1/F_0, the ratio of the first harmonic component to the mean elevation of the neuronal response to a drifting sinusoidal grating stimulus, another indicator of simple ($F_1/F_0 > 1$) or complex ($F_1/F_0 < 1$) cells. We modeled a simple condition that a V1 neuron receives dominant inputs from ON and OFF afferents for two cases in Fig. 2d. In both cases, ON and OFF RGCs produce sinusoidal responses, but they can induce either constructive or destructive summation of responses, depending on ON/OFF subregions distance (Fig. 2e, top). This will generate distinct level of modulation of membrane voltage responses in V1 (Fig. 2e, middle), and thus the instantaneous firing rate of the model V1 neuron is either strongly modulated ($F_1/F_0 > 1$, simple cell) or weakly modulated ($F_1/F_0 < 1$, complex cell) depending on the spatial arrangement of ON and OFF feedforward afferents (Fig. 2e, bottom). Based on the spike rectification model (Mechler & Ringach, 2002; Priebe et al., 2004), a nonlinear sigmoidal transfer function between the ON–OFF distance of RF and the F_1/F_0 of neural response was obtained analytically (Fig. 2f, see Methods). From this result, we confirmed that the unimodal distribution of the ON–OFF distance shown in Fig. 2c can generate bimodal segregation of F_1/F_0 observed in the monkey data (Fig. 2g).

Note that the current model predicts the coexistence of both simple and complex cells in the thalamo-recipient layer (as observed in Martinez et al. (2005)), regardless of the bimodality of the distribution of F_1/F_0. Previously, it was suggested that the bimodal distribution of the F_1/F_0 ratio can be considered as evidence that simple and complex cells are distinct classes of V1 neurons (Skottun et al., 1991). However, more recent studies have shown that whether the distribution is bimodal or unimodal does not necessarily imply distinct classes but can be a by-product of the nonlinearity of the measure. For example, although the distribution of F_1/F_0 is bimodal in the monkey V1, the underlying membrane voltage measures (V_1/V_0) were unimodally distributed and the shape of the distribution was dependent on an intracortical parameter, such as the spike threshold (Mechler & Ringach, 2002; Priebe et al., 2004). Our model can readily account for various conditions of the F_1/F_0 distribution, such as a simple cell being more dominant than complex cells, as in the cat V1 (Supplementary Figure 1).

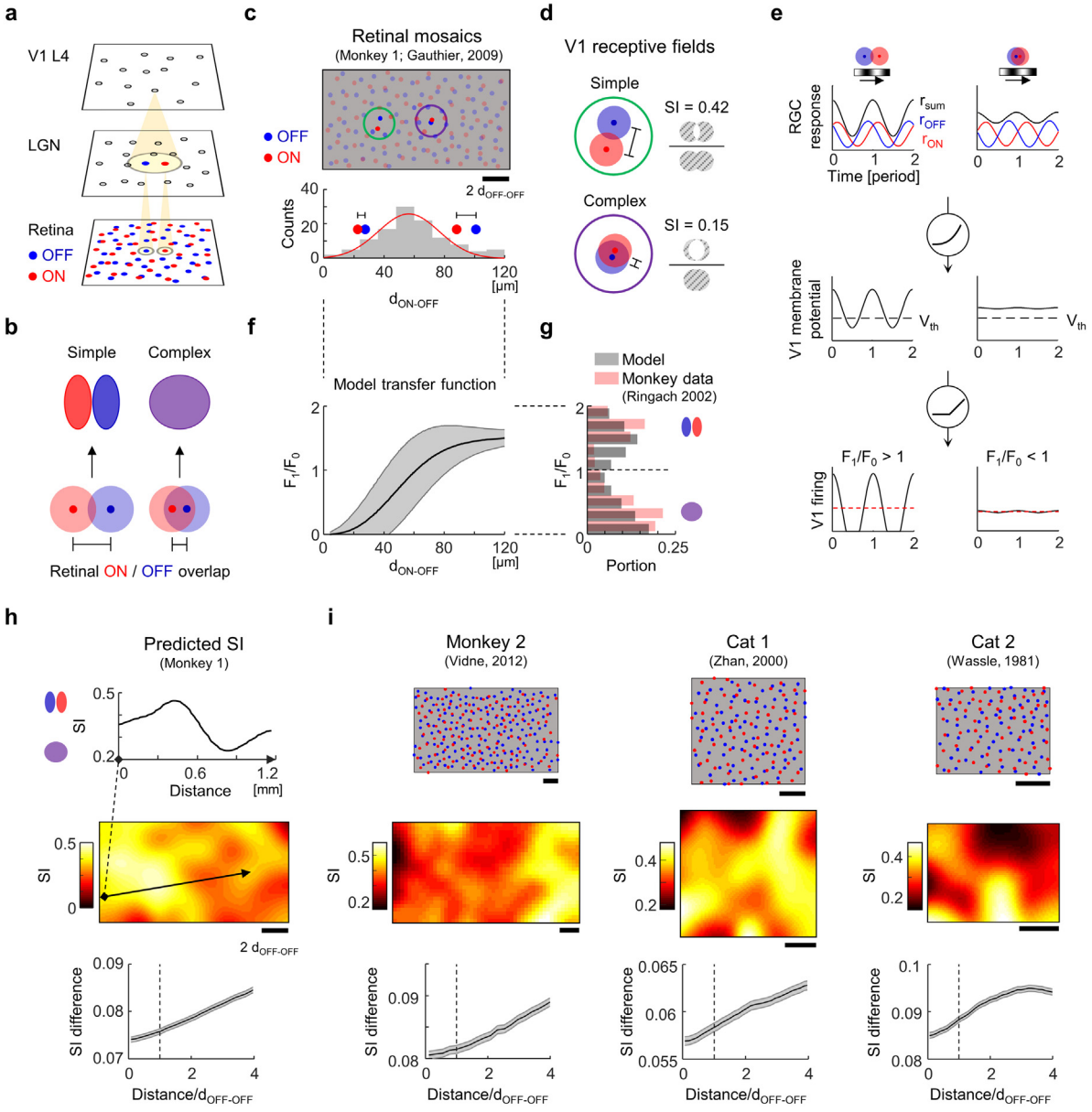

Fig. 2. Retinal-origin model of simple and complex cells. (a) Illustration of the feedforward projections from ON and OFF retinal mosaics to V1 (b) The retinal origin model of simple and complex cells. (c) ON and OFF-center RGC receptive field mosaic data from monkeys (Gauthier et al., 2009). Red and blue dots represent the center of mass. Scale bar indicates $2d_{OFF\text{-}OFF}$. ON–OFF dipoles (N = 116) were defined as a line from each OFF cell to the nearest ON cell, and $d_{ON\text{-}OFF}$ denotes the size of the dipole. Bottom histogram represents the distribution of $d_{ON\text{-}OFF}$, fitted to a Gaussian (Red curve). (d) Example receptive fields of local ON and OFF RGC afferents (from green and purple circles in b). Simpleness index (SI) measures the spatial segregation between ON and OFF receptive field sub-regions. (e) Illustration of responses of RGCs and V1 neurons to the drifting grating stimulus (see Methods). Dashed black line (V_{th}) represents spike threshold. Dashed red line represents mean response. (f) A nonlinear transformation between F_1/F_0 and ON–OFF distance obtained by an analytic model (see Methods). Shaded area represents standard deviation. (g) Resulting bimodal distribution of F_1/F_0 predicted by the model (gray, Hartigan's dip test, $p < 10^{-5}$) is compared with the histogram of F_1/F_0 in Fig. 1c (red). (h) Top, sample 1-D profile of SI obtained from mosaic data in (c). Middle, spatial map of estimated SI. Bottom, the average difference of SI between two arbitrary points as a function of distance (from 10,000 pairs of randomly sampled points). Black dashed line indicates the size of smoothing filter used to obtain the SI map. (i) Same analysis for three different mosaics data. Shaded areas represent SEM. (For interpretation of the references to color in this figure legend, the reader is referred to the web version of this article.)

2.2. Periodic clustering of simple/complex neurons from RGC mosaics

One important prediction arises from the result above: the spatial organization of simple and complex cells across a thalamo-recipient layer would reflect the spatial layout of the corresponding RGC mosaic and therefore would be organized into topographical clusters. As shown in Fig. 2h, the spatial distribution of SI estimated from the RGC mosaics is clustered across the space, generating local regions of large or small SI values. As a result, the difference of SI between two points in the RGC mosaics gradually increases as the two points become farther apart, implying spatial clustering of SI across the retinal mosaics (Fig. 2h, bottom). We repeated this analysis for four sets of RGC mosaic data of monkeys and cats, confirming the spatial clustering of SI (Fig. 2i, monkey 2 Vidne et al., 2012, cat 1 Zhan & Troy, 2000, cat 2 Wassle et al., 1981). This finding predicts that simple and complex cells in V1 would appear as an organization of clusters across a thalamo-recipient layer.

Previous theoretical studies showed that quasi-periodic maps of orientation tuning may arise from the spatial organization of

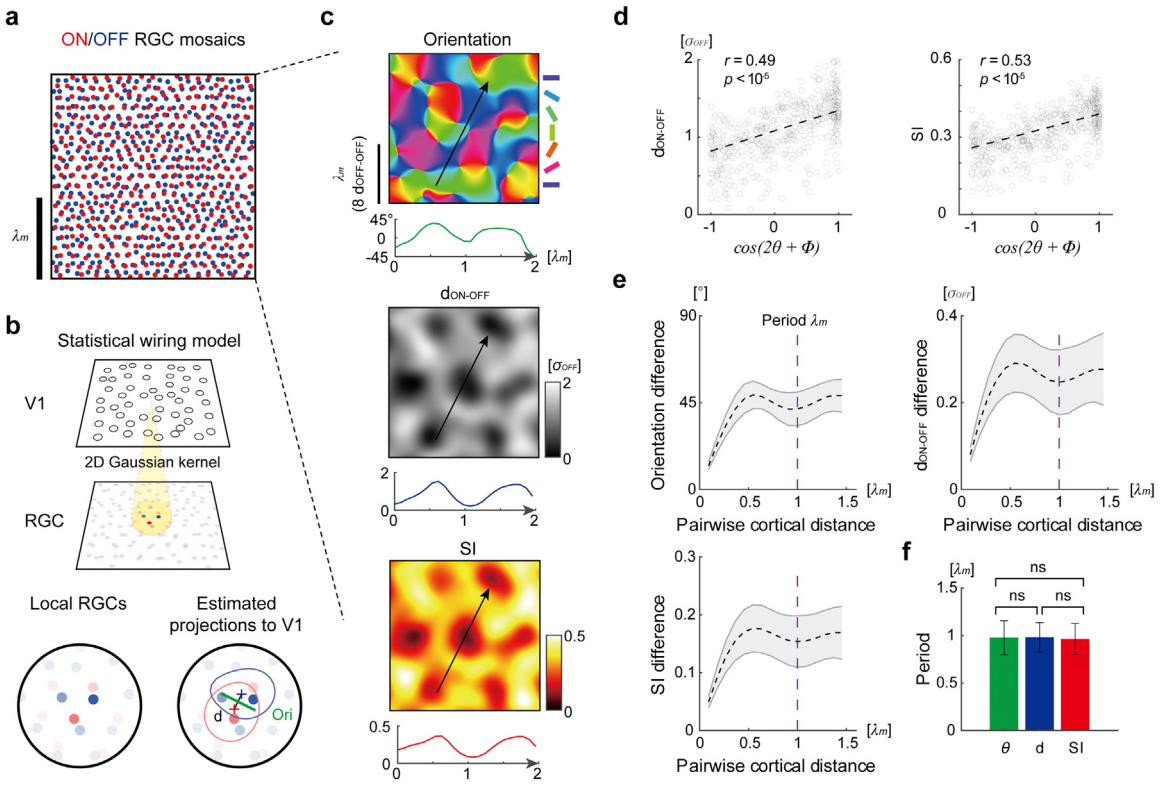

Fig. 3. Moiré interference of retinal mosaics predicts the periodic spatial organization of SI, $d_{ON\text{-}OFF}$, and orientation preference in V1. (a) ON- (red) and OFF-center (blue) retinal ganglion cell receptive field mosaics are described as two noisy hexagonal lattices with different periodicity and the same angle. The resulting hexagonal moiré interference pattern has a characteristic period λ_m. (b) Illustration of the statistical wiring model and example estimated projections to V1 from local RGCs. Red and blue crosses represent the center of ON and OFF subregions, respectively. (c) Pseudo color representation of the synthetic map of preferred orientation, $d_{ON\text{-}OFF}$, and SI (with example 1-D profiles along black arrow). σ_{OFF} represents the RF size of model OFF RGCs. Scale bar indicates λ_m ($= 8d_{OFF\text{-}OFF}$). (d) Correlation between cosine of orientation ($\cos(2\theta + \Phi)$) and $d_{ON\text{-}OFF}$ (left), and SI (right) obtained from diverse cortical penetrations on model maps (N = 100 penetrations). (e) Pairwise differences of orientation (top), $d_{ON\text{-}OFF}$ (middle), and SI (bottom) for the simulated model maps. The common period λ_m is denoted as a purple dashed line. Shaded gray areas represent the standard deviation obtained from different cortical penetrations. (f) Consistent periods obtained from three maps (one period value for each penetration for each map, N = 100 penetrations). ns: not significant (Wilcoxon rank-sum test, $p = 0.97, 0.72, 0.68$, for SI - orientation, SI - $d_{ON\text{-}OFF}$, $d_{ON\text{-}OFF}$ - orientation, respectively). Error bars indicate the standard deviation. (For interpretation of the references to color in this figure legend, the reader is referred to the web version of this article.)

RGC mosaics (Jang & Paik, 2017; Jang et al., 2020; Paik & Ringach, 2011; Ringach, 2004, 2007; Soodak, 1987). Combining this notion with our model, we suggest that simple/complex tuning changes periodically across the cortical surface as orientation tuning: In the Paik–Ringach model (Paik & Ringach, 2011, 2012), it was suggested that two noisy hexagonal lattices of ON and OFF RGC mosaics generate a periodic interference pattern of a local ON–OFF dipole-like arrangement, called a moiré interference pattern (Fig. 3a). In this interference pattern, the ON–OFF distance and ON–OFF angle changes periodically across the mosaics, with their spatial period denoted as λ_m. As suggested in previous model studies (Ringach, 2004, 2007), we assumed that the response of a local V1 neuron is constrained by the structure of ON/OFF afferents from the RGC mosaics: Considering that cortical neurons receive feedforward inputs from multiple RGCs relayed by LGN neurons (Alonso et al., 2001), the structure of ON/OFF subregions was estimated by sampling the receptive field of ON and OFF RGCs within a retinal area that match the retinotopic location of a target V1 neuron (Fig. 3b, see Methods for details). In this scenario, orientation tuning can be estimated from the alignment of ON and OFF subregions projected from local RGCs, and the SI of a V1 neuron can be estimated from the segregation between ON and OFF subregions of corresponding afferents.

Our model simulation predicts that the preferred orientation, $d_{ON\text{-}OFF}$, and SI, of V1 neurons are organized into a spatial cluster of the same period, λ_m (Fig. 3c). All three of the simulated maps showed clear periodic clustering of tuning across the cortical surface, matching the periodic organization of the RGC interference pattern. Structural similarity between the periodic clustering of different tunings was estimated from the maximum correlation measured at random locations sampled across the cortical surface (N = 10,000). Cortical profiles of $d_{ON\text{-}OFF}$ and SI in the model showed strong correlation with the cosine of the orientation preference (Fig. 3d). In position-shuffled control, the probability of obtaining as high a correlation value as in the model was significantly low ($p < 0.0001$ for both $d_{ON\text{-}OFF}$ and SI). Furthermore, the period of each map, calculated from average pairwise difference as a function of pairwise distance, was identical to the predicted period λ_m of the retinal moiré interference (Fig. 3e). The distribution of the obtained period values of orientation, $d_{ON\text{-}OFF}$, and SI from different locations of the model map were statistically indistinguishable (Fig. 3f). Furthermore, these common periodicity outcomes of the orientation, $d_{ON\text{-}OFF}$, and SI were similarly observed in the measured mosaics (Supplementary Figure 3), and this tendency might be confirmed when sufficient data pertaining to multiple mosaics with similar levels of eccentricity in higher mammals (cats or monkeys) become available from future studies.

Next, we conducted an additional analysis to test the robustness of the model with variations of the number of ON and OFF inputs seeding the receptive fields. Specifically, we sought to determine the highest effective number of RGC inputs with which our model can operate. For simplicity, we sampled N

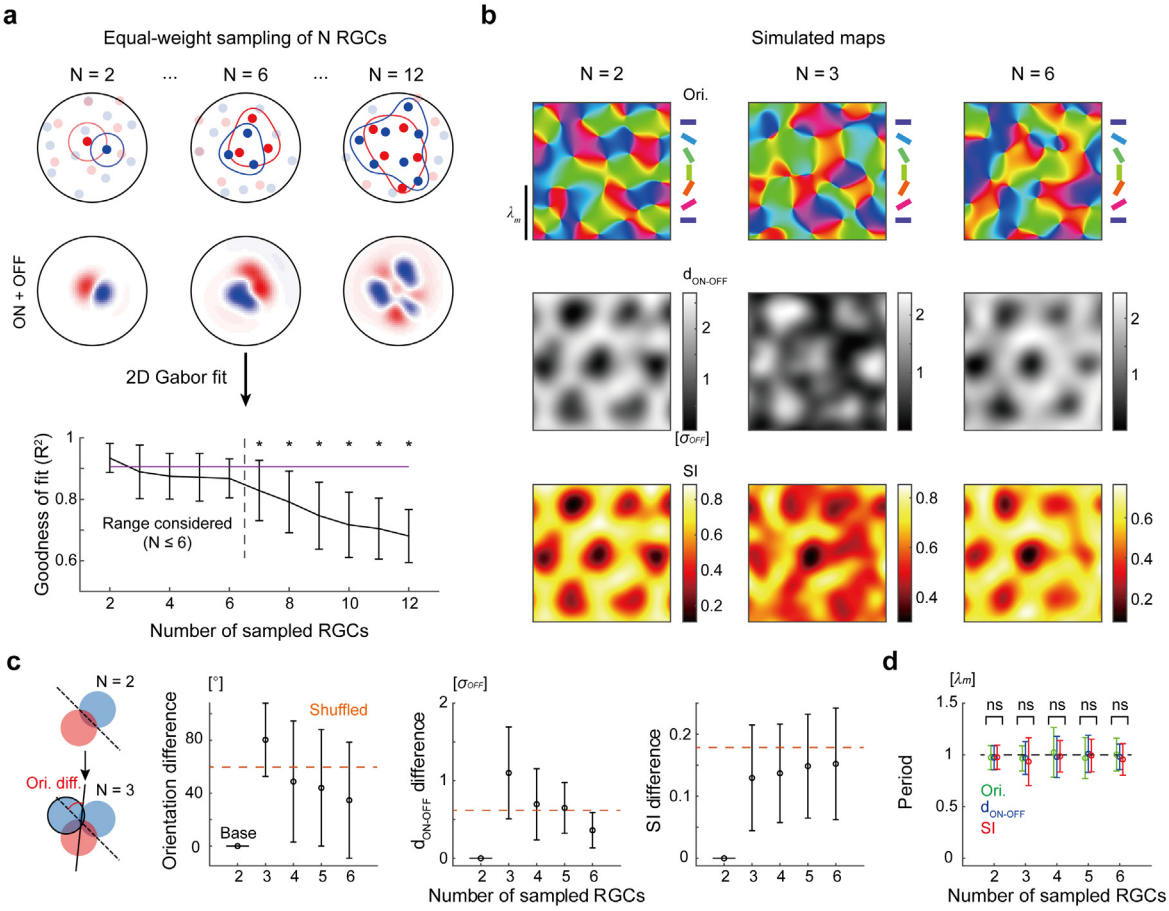

Fig. 4. Robustness of the model under the variation of the number of sampled RGCs. (a) (top) Sampling N nearest-neighboring RGCs with equal weights to generate the receptive field of a neuron in V1. Example receptive fields for N = 2, 6, 12 are shown. (bottom) Goodness of fit of induced V1 receptive fields to 2D-Gabor function (Ringach, 2002) when varying the number of sampled RGCs. The purple line indicates the value estimated from data in monkeys (Ringach, 2002). The goodness of fit is significantly different from that reported in animal data if N exceeds six (One-tailed, two-sample t-test, p = 0.98, 0.14, 0.017, 0.010, 0.0032, 2.5×10^{-6}, 6.6×10^{-11}, 2.2×10^{-16}, 3.2×10^{-21}, 3.0×10^{-24}, and 1.9×10^{-30} for N = 2 – 12 respectively; The star indicates that p<0.001) (b) Simulated maps of the preferred orientation, $d_{\text{ON-OFF}}$, and SI when varying the number of sampled RGCs. (c) (left) A simple toy model in which the addition of one ON (or OFF) RGC input can significantly modulate the structure of the ON and OFF domains in the receptive field. (right) Changes of the orientation, $d_{\text{ON-OFF}}$, and SI values when the number of sampled RGCs, N, increases (N = 3–12). Dashed line indicates changes of those in shuffled maps of N = 2. (d) Consistency of the spatial period observed from each map (ns: not significant, Wilcoxon rank-sum test, from the left, p = 0.74, 0.93, 0.80, p = 0.85, 0.92, 0.98, p = 0.43, 0.36, 0.93, p = 0.11, 0.62, 0.14, p = 0.35, 0.21, and 0.92, for SI - orientation, SI - $d_{ON\text{-}OFF}$, and $d_{ON\text{-}OFF}$ - orientation, respectively). Error bars indicate the standard deviation in (a), (c), and (d)

nearest-neighboring RGCs (regardless of the ON/OFF sign) with the same weight for each specific position of V1 (Fig. 4a, top). We initially examined the profile of the receptive fields generated by N nearest-neighboring RGCs. We calculated the goodness of fit (R^2) of the receptive field to the 2D Gabor wavelet function (Ringach, 2002) to find the range of N within which a biologically observable structure of the V1 receptive fields is generated. We found that the structure of the induced V1 receptive fields becomes significantly different from that reported in animal data if N is larger than six at the significance level of 0.001 (Fig. 4a, bottom). This result is consistent with or similar to the conditions reported in previous model studies (Paik & Ringach, 2011; Ringach, 2004, 2007; Song et al., 2021). Next, we simulated a map of the preferred orientation, $d_{\text{ON-OFF}}$, and SI again (Fig. 4b). We observed that the local tunings vary as soon as the number of sampled RGCs increases from two (Fig. 4c). However, we found that the periodic topography of the induced maps remains consistent under this variation (N = 2–6). Accordingly, our key result, that the preferred orientation, $d_{ON\text{-}OFF}$, and SI of V1 neurons are organized into a spatial cluster with a similar period, was found to be consistent across all conditions tested here (N = 2–6, Fig. 4d). Notably, the observed spatial periods of the maps were consistent with the characteristic period of the retinal mosaic (λ_m). This result implies that the periodic structure of the retinal mosaic can still provide a common source of such periodic maps in V1, even when the neuronal tuning of local maps is modulated to some degree as N increases.

2.3. Periodic spatial organization of simple/complex cells

In the previous section, we showed that our model predicts a correlation between simple/complex tuning and underlying orientation tuning across the cortical surface. To validate this model prediction with biological data, spatial organization of simple and complex receptive fields in V1 was examined using published receptive field data (Kremkow et al., 2016) obtained by multielectrode recording in cats (Fig. 5a). From the observed ON and OFF receptive fields, the simple/complex tuning index (SI) and the distance between ON/OFF center of mass ($d_{ON\text{-}OFF}$) of each recording site were measured (Fig. 5b). The recording data contained both simple- and complex-like receptive fields, which showed segregated (left) or overlapped (right) ON and OFF sub-regions respectively. As reported (Kremkow et al., 2016), the distribution of orientation preference varied periodically (Fig. 5c, top). Interestingly, both the spatial variation of $d_{ON\text{-}OFF}$ and SI

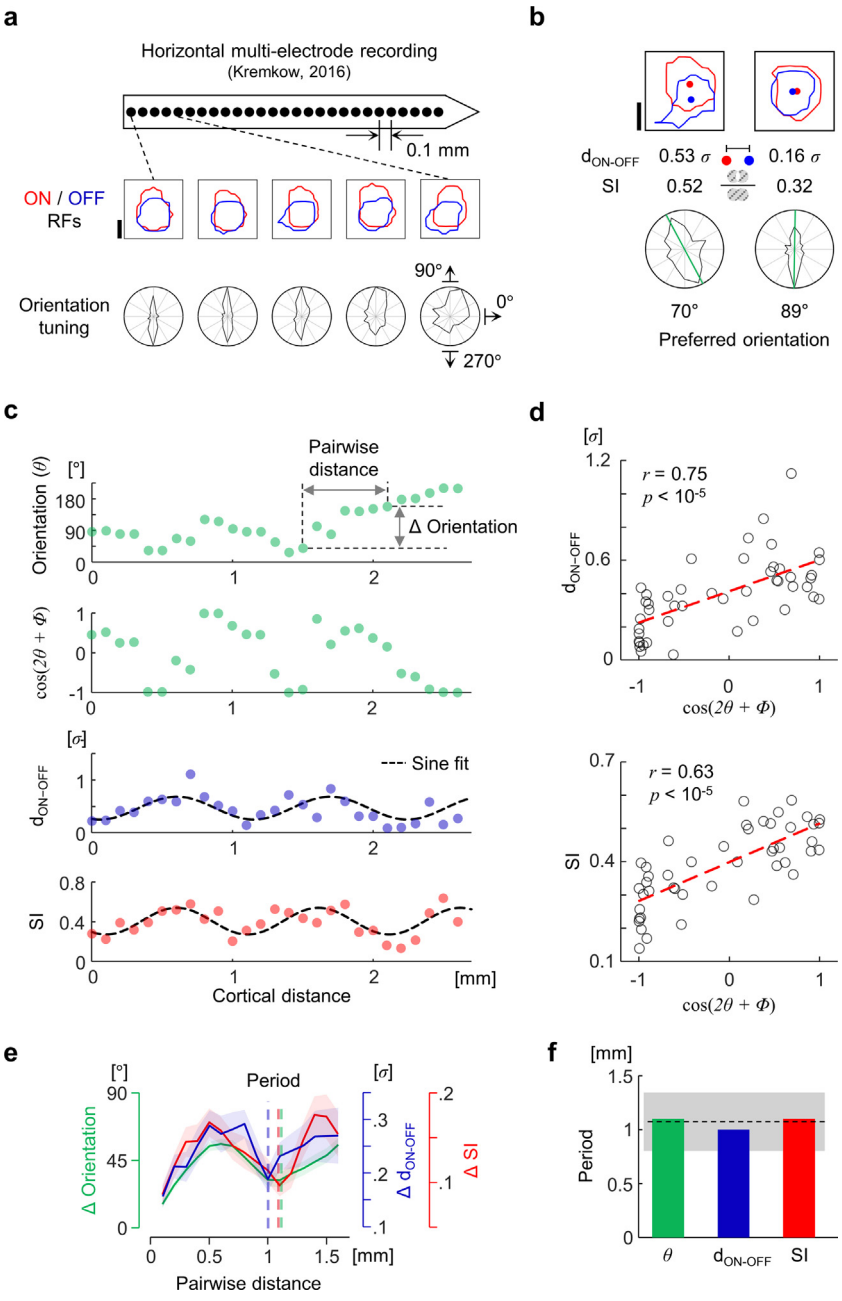

Fig. 5. Periodic spatial organization of simple/complex receptive fields and the common period with orientation preference in cat V1. (a) Illustration of multielectrode recording from the reference (Kremkow et al., 2016). The contour of ON and OFF receptive fields (measured with light and dark stimuli, respectively) is defined as a level of z-score = 1.5 for each ON/OFF receptive field. Scale bar: average radius (σ) of the ON/OFF receptive field for each penetration. Polar plots represent a normalized response to drifting bars. (b) Example calculation of $d_{ON\text{-}OFF}$ (distance between center of mass of ON/OFF sub-regions), SI, and preferred orientation. (c) Periodic spatial clustering of orientation preference (green, and its phase-adjusted cosine values), $d_{ON\text{-}OFF}$ (blue), and SI (red). The Black dashed lines are sine fits for $d_{ON\text{-}OFF}$ and SI. The $d_{ON\text{-}OFF}$ fit: $0.47 + 0.22 \times \sin(2\pi x/\lambda - 1.92)$, $\lambda = 1.1$ mm ($R^2 = 0.41$, $p = 3\times10^{-4}$). The SI fit: $0.4 + 0.13 \times \sin(2\pi x/\lambda - 2.19)$, $\lambda = 1.0$ mm ($R^2 = 0.52$, $p = 2\times10^{-5}$). Phase difference between two fits: 17°. (d) Correlation between cosine of orientation ($\cos(2\theta + \Phi)$) and $d_{ON\text{-}OFF}$ (top), and SI (bottom) (2 penetrations, N = 52 sites). (e) Average pairwise difference as a function of pairwise distance (averaged over 2 penetrations, averaged pairwise sample > 20 for each pairwise distance). Shaded areas represent SEM. Dashed vertical lines represent the period of each curve (~1.1 mm). (f) Comparison of the observed period of SI, $d_{ON\text{-}OFF}$, and orientation with reported values of the orientation map periods (black dash line and shaded area, 1.07 ± 0.27 mm, N = 186; Rao et al., 1997). (For interpretation of the references to color in this figure legend, the reader is referred to the web version of this article.)

in V1 appeared periodically clustered along the cortical penetrations. The distribution of $d_{ON\text{-}OFF}$ (Fig. 5c, 3rd row) was well-fitted to a sinusoidal function of ~1.1 mm period. Comparable to this, the distribution of SI (Fig. 5c, bottom) was also fitted to a sinusoidal function of nearly identical spatial period (~1.0 mm) and phase (phase difference ~17°). We found that the value of the observed SI and $d_{ON\text{-}OFF}$ was tightly correlated (N = 52 data points from 2 penetrations, Pearson correlation coefficient, $r = 0.66$, $p = 1.2\times10^{-7}$).

Obviously, the correlation between $d_{ON\text{-}OFF}$ and SI can be expected in most cases due to their spatial relationship. However, as the receptive field data are noisy in animal data, the two measures are not always perfectly correlated (Mata & Ringach, 2005). Thus, it is possible that a periodic organization will be observed more readily or more precisely in one of the two measures. In addition, the degree of structural irregularity of the receptive field structure (Gauthier et al., 2009) can also affect the precision of the periodicity measurement. To address all of these possible issues,

we performed further analyses to examine whether a significant modulation of the relationship between $d_{\text{ON-OFF}}$ and SI can be observed due to the variations of the receptive field structure and of their spatial alignment (Supplementary Figure 4). As a result, we found that the correlation between $d_{\text{ON-OFF}}$ and SI is consistently observed under various conditions of receptive fields in which the spatial structure and the alignment of the ON and OFF receptive fields were varied, as observed in animal data. This suggests that both measures can be used for estimations of periodic organizations under various conditions.

As predicted by the model, the spatial organization of $d_{ON\text{-}OFF}$ and SI was correlated with orientation preference, and had a common period identical to that of the orientation. As shown in Fig. 5d, the values of $d_{ON\text{-}OFF}$ (or SI) and the cosine of orientation preference (Fig. 5c, 2nd row) were correlated across cortical surface (N = 46 data points from 2 penetrations). In position-shuffled control, the probability of obtaining as high a correlation value as in the data was significantly low ($p = 0.0026$ for $d_{ON\text{-}OFF}$ and $p < 0.0001$ for SI). Furthermore, the remarkably similar clustering period among the three organizations was manifested in the average absolute pairwise difference for each measure (orientation, $d_{ON\text{-}OFF}$, and SI) plotted as a function of cortical distance (Fig. 5e, averaged over the 2-penetration data sets, where each mean value includes more than 20 pairwise comparisons). The calculated mean period values (orientation 1.1 mm, $d_{ON\text{-}OFF}$ 1.0 mm, SI 1.1 mm) were not only similar to each other, but also matched the previously reported values of period of orientation maps in cats (Rao et al., 1997) (Fig. 5f). These findings – the periodic organization of simple/complex receptive fields and a spatial period consistent with orientation tuning maps – imply that our retinal origin model can account for the relationship between the spatial clustering of simple/complex tunings and the orientation maps in V1.

As it has been reported that the value of F_1/F_0 is significantly correlated with the overlap of the ON/OFF receptive field (Mata & Ringach, 2005), a periodic organization of F_1/F_0 is also predicted from the observation of the periodic organization of SI. Our simulation using a linear–nonlinear model with the observed ON and OFF receptive field data suggests that F_1/F_0 is also expected to have a periodic spatial organization in V1 (Supplementary Figure 5). Further validation using a direct measurement of F_1/F_0 with a large dataset is necessary to confirm this model prediction.

In addition, to strengthen the model prediction of the topographic correlation between orientation tuning and simple/complex tuning in the experimental data, we conducted an additional analysis of the multi-electrode data and observed that the extrema of the simpleness and the pinwheel positions in the orientation map spatially overlap, as our model predicts (Supplementary Figure 6). Specifically, our model predicts that the locations of pinwheels are likely to be either on the maxima or minima of the local simple/complex tuning (or SI) due to the topographic matching between the ON–OFF distance in the moiré interference pattern and the corresponding orientation map. We examined the experimental data and found that the SI values are either maxima or minima at the pinwheel locations, similar to the model analysis. This result suggests the possibility that our model can exploit the information of the orientation map topography to predict local simple/complex tunings, further supporting the validity of the model.

3. Discussion

Our findings suggest that simple and complex tuning in V1 can commonly originate from spatial arrangement of the local projection of retinal afferents. An analysis of multi-electrode recording data from cats shows a tendency consistent with the model prediction that simple and complex receptive fields are periodically clustered in V1. Moreover, the observed periodic organization has a period consistent with the orientation preference, implying the common origin of the simple/complex and the orientation tuning in V1. The Paik–Ringach model provides a possible explanation for the observed periodicity from the periodic projection of retinal afferents imprinted in retinal mosaics.

Our simplified model is designed to consider RGC cells as only inputs based on the concept that the receptive field of a V1 neuron at the early developmental stage is restricted by the structure of the receptive fields of local ON and OFF RGCs (Jin et al., 2011) and that intracortical inputs from other V1 cells may refine this crudely initialized tuning successively. Specifically, this assumption is based on the previous experimental observation that orientation-selective neurons and their orderly cortical structures are observed before the complete development of intracortical circuits (Crair et al., 1998), and that cortical receptive fields are strongly constrained by feedforward thalamic afferents (Jin et al., 2011). Notably, it was reported that the orientation preference of a cortical column can be predicted by the local arrangement of ON/OFF afferents (Lee et al., 2016) and that other functional tunings such as direction selectivity (Lien & Scanziani, 2018), ON/OFF polarity, and ocular dominance (Kremkow et al., 2016) are observed to develop from the integration of thalamic feedforward inputs.

Based on these observations, our model assumes that the initial cortical phase invariance is restricted by the spatial structure of the ON and OFF feedforward afferents, especially before the intracortical circuit is fully developed by visual experience. This notion is in line with a number of our previous publications that explain the retinal origin of the functional organization of the early visual cortex — including orientation maps, ocular dominance maps, spatial frequency maps, and their orthogonal relationships (Jang & Paik, 2017; Jang et al., 2020; Paik & Ringach, 2011, 2012; Song et al., 2021). However, it is important to note that the current model is not a complete description of cortical development. Extension of the current concept with additional factors such as intracortical interactions and refinement with visual experience is necessary, as such work will address more realistic issues in adult animals (Lien & Scanziani, 2013) that feedforward afferents alone cannot explain.

Several works suggest that the nonlinear summation of simple cell-like linear filters can generate the phase-invariant orientation tuning properties of complex cells. For example, the phase-invariant responses of a complex cell were modeled as a nonlinear summation of the responses of simple cells with opposite phases (Adelson & Bergen, 1985; Touryan et al., 2005). More recently, revised models using a combination of various linear filters and nonlinearities have been presented to capture the wide variation of the observed phase invariance in V1 cells (Almasi et al., 2020; Rust et al., 2005; Sharpee et al., 2004). However, it is notable that simple and complex cells are observed even at the early developmental stage and that their proportions are similarly maintained throughout the visual experience (Albus & Wolf, 1984; Braastad & Heggelund, 1985). Furthermore, considering that orientation-selective neurons and their orderly cortical structures are observed before the complete development of intracortical circuits (Crair et al., 1998), early feedforward inputs may provide a blueprint for such an architecture. Our result suggests that such simple and complex receptive fields can be initialized in parallel by the structure of the ON and OFF feedforward afferents, particularly before the intracortical circuit is fully developed. However, it should be noted that our model does not preclude a scenario of 'serial' development, in which complex cells develop from the nonlinear integration of the input of simple cells (Adelson & Bergen, 1985; Touryan et al., 2005). Rather, our model suggests a probable scenario of the 'parallel'

development of both simple and complex cells, in line with our recent studies on the development of various cortical tunings in V1 (Song et al., 2021).

In previous studies on cats, it was reported that simple cells are mostly observed in layer 4 of V1 (Hirsch et al., 1998; Martinez et al., 2002), and that the proportion of complex cells becomes greater as the layers become deeper (Martinez et al., 2005). These observations are not different from our model prediction, because projection from an input layer of V1, especially layer 4, will converge into a superficial layer, such as layer 2/3, to generate more complex receptive fields. In our model, the retinotopic overlap between simple and complex cells across the layer (Alonso & Martinez, 1998) can also arise from convergent feedforward projections between the layers. Although hierarchical variation of simple/complex tuning has been extensively discussed since the pioneering study of Hubel and Wiesel (1962), how both types of cells can arise in V1 is not fully understood. Here we focus on the complex cells that coexist with simple cells (almost equal populations) in layer 4 of monkeys, which receives the majority of feedforward afferents from the thalamus (Ringach et al., 2002). Even in layer 4 of cat, which consists mostly of simple cells, a significant portion of the complex cells were observed and simple cells exhibited various degrees of nonlinearity, as did the complex cells (Carandini & Ferster, 2000; Priebe et al., 2004). Our model suggests a possible scenario for the parallel development of simple and complex cells in the thalamo-recipient layer.

Our current study provides a conceptual model of a probable developmental scenario, but it must be noted that currently available experimental data for validation of the model is very limited. Thus, the suggested developmental scenario will need to be fully validated by further experimental observations involving information about both the neuronal receptive fields and cortical positions of large populations of neurons in the visual cortexes of young animals. A recent study demonstrated that such information can be procured from large-scale two-photon imaging data (Lee et al., 2016). Although such a dataset is not immediately available, it would be possible to identify a two-dimensional map of simple and complex cells in the V1 in higher mammals (cats or monkeys) in future studies for validation of the current model. Previous works also suggested that wide functional variation of complex cell properties can be reproduced by unsupervised learning with the temporal slowness principle (Berkes & Wiskott, 2005; Wiskott & Sejnowski, 2002). Our current model only considers feedforward circuits as a simplified model of the early developmental process of the visual cortex, but consideration of additional factors, such as intracortical connectivity and the spatiotemporal dynamics of receptive field, would enable the model to account for more realistic characteristics observed in experimental data. For example, consideration of the simple temporal delay between the ON and OFF pathways along with our current model can readily address "direction selectivity". It is notable that our recent publication (Song et al., 2021) discusses this issue in detail using the same model framework; in the current model that only considers static receptive fields, direction selectivity of V1 neurons can be seeded by simply considering the intrinsic temporal delay between ON and OFF retinal projections. In this scenario, the delay between the ON and OFF response induces a more or less synchronized response of the V1 target neuron depending on the direction of the drifting grating stimulus.

The current model is also limited in its ability to address "end and side inhibition", referring to a property of V1 neurons that shows sensitivity to the length and width of the stimulus, respectively (DeAngelis et al., 1994). These properties are considered to stem from the inhibitory inputs outside the classical receptive fields of the neurons (Seriès et al., 2003), but the current model does not consider any mechanism regarding extra-classical receptive fields. However, it is possible to address this issue in the model by including inhibitory horizontal connectivity in V1 so that the response of an orientation-tuned neuron is inhibited by inputs from other V1 neurons with the same orientation preference beyond the classical receptive field of the neuron. In addition, consideration of intracortical interactions may explain the variation of the sharpness of the orientation and frequency tuning curves. Previous studies reported that the orientation preference angle of a V1 neuron can be predicted by the structure of the feedforward thalamic input (Kremkow et al., 2016; Lee et al., 2016), whereas the tuning can be modulated by a number of factors, such as the spike thresholds of individual neurons (Carandini & Ferster, 2000; Mariño et al., 2005) and intracortical interactions (Lee et al., 2012; Li et al., 2013; Lien & Scanziani, 2013). Therefore, consideration of these additional factors may enable our model to implement more realistic characteristics. Overall, it should be noted that our model can predict the global topography of orientation maps and simple/complex maps but is limited if used to estimate the precise tunings of individual neurons.

Another limitation of the model is that it targets a single pathway, especially the magnocellular pathway (parasol retinal ganglion mosaic), which would seed the initial tuning of V1 neurons by providing the earliest inputs. Specifically, previous works suggested that orientation selectivity in the cat V1 is observed between developmental stages E57 and P0, but only in sublayer 4Cα, which receives dominant inputs from the magnocellular pathway (Ghosh & Shatz, 1992; Mooser et al., 2004; Shatz & Luskin, 1986). On the other hand, the migration of cortical cells in layers 2/3, which receive dominant inputs from the parvocellular pathway, is completed at postnatal week 3. This suggests that the initial orientation tuning in V1 layer 4 is dominantly governed by the inputs from the magnocellular pathway. Hence, we inferred that the cortical tuning as well as the associated topographic map are initially seeded by this single type of RGC that develops earlier, while the connections of other types of cells could be fitted into this blueprint via activity-dependent plasticity. However, this is only an assumption in the current model, and further experimental studies that reveal the precise contributions of different types of RGCs during the development of functional maps may contribute to the revision of the current model.

The periodic organization of simple and complex cells can induce an efficient structure that includes the complete set of simple-complex (or phase-specific/invariant) tunings along with other visual features. Previous studies suggested that when multiple features of V1 neurons (such as orientation, spatial frequency, and ocular dominance) change in a similar period and their gradients intersect orthogonally, "efficient tiling" can be achieved so that all combinations of multiple features can be efficiently encoded within a cortical hypercolumn (Nauhaus et al., 2016; Song et al., 2021; Swindale et al., 2000). When the periods of phase invariance and orientation maps are similar, as suggested in the current model, efficient tiling between the phase invariance and other tunings can also be obtained together. A recent study (Song et al., 2021) reported that such efficient tiling can originate from the structure of the retinal mosaic and that the gradient of the ON–OFF distance intersects perpendicularly the gradient of the ON–OFF angle seeding the orientation tuning. Furthermore, as neurons in earlier layers can be combined in a further layer by nonlinear processing, such a spatial distribution of the phase invariance can be more uniform in deeper layers. Previously, as the spatially biased architecture of orientation preference is widely observed in V1 (e.g., the iso-orientation domain), it was postulated that "orientation scotomas" may exist — the cortex cannot encode every orientation equally well at some locations

(Paik & Ringach, 2011). In this scenario, this type of biased encoding of a specific visual feature (e.g., orientation, phase invariance) in the thalamo-recipient layer can be supplemented through further feedforward and recurrent connections, and the periodic organization of early layers may help to induce a uniform mixture of complete feature sets in further layers. Overall, our results suggest that projection of the structure of the retinal mosaic to the early thalamo-recipient layer would play a role in providing a layout for efficient visual processing.

4. Conclusions

Our finding suggests that the architecture of V1 is not only hierarchical, but also parallel, and that this parallel architecture refines the classical notion of visual cortex. That is, the role of simple/complex cells in visual information processing is not restricted to distinguishing different stages of the cortical microcircuits, but can be regarded as an element of functional diversity in the same cortical layer.

To sum up, the observed periodic spatial organization of simple and complex receptive fields provides a population-level clue regarding how simple and complex receptive fields may arise initially. Furthermore, it leads to the view that the spatial organization of ON and OFF retinal afferents can contribute significantly to the simple/complex neural response spectrum in V1. Complementary to the classical notion that simple and complex receptive fields are hierarchically distinct, the observed periodic spatial organization of simple/complex receptive fields shows systematic variation in layer 4 of V1, which receives thalamic inputs. That the period is consistent with that of the orientation preference encourages the view that structured retinal afferents designed by interference between ON and OFF RGC mosaics provide the common source of both orientation preference and the simple/complex-property of the connected V1 neurons. These results support the scenario that the diverse functional tunings of V1 can be initially biased by the arrangement of ON/OFF afferent inputs of retinal origin.

5. Methods

5.1. Simpleness index (SI)

To quantify the simple/complex tuning of the receptive field, we calculated the simpleness index (SI), which represents the degree of segregation between ON/OFF subregions (Dean & Tolhurst, 1983; Lee et al., 2016; Mata & Ringach, 2005; Van Hooser et al., 2013). The SI is defined as follows:

$$SI = \frac{\sum |RF_{OFF} - RF_{ON}|}{\sum |RF_{OFF} + RF_{ON}|}$$

where RF_{OFF} and RF_{ON} represent 2-d matrices of ON and OFF receptive field subregions, respectively, and the summation is over all matrix elements. Note that the relationship between $d_{ON\text{-}OFF}$ and SI is dependent on the shape and size of the ON and OFF receptive fields.

5.2. Analysis of RGC mosaics

The ON–OFF dipole was defined as a line connecting the nearest ON cell from each OFF cell in the mosaic. The SI values in Fig. 2 were calculated by assuming that a model V1 neuron receives dominant inputs from one ON-center RGC and one OFF-center RGC of equal strength. The receptive field of ON- and OFF-center RGCs was modeled as the difference of a Gaussian ($\sigma_{surround} = 3\sigma_{center}$, $\sigma_{center,ON/OFF}$ = half of the average ON–ON/OFF–OFF distance, respectively). The map of SI in Fig. 2h and i was obtained as,

$$SI(\boldsymbol{r}) = \sum_i SI_i * exp(-\frac{\left|\boldsymbol{r} - \boldsymbol{r}_{dipole,i}\right|^2}{2\sigma_r^2}),$$

where $\boldsymbol{r}_{dipole,i}$ and SI_i are the center and SI value of the *ith* dipole, respectively (σ_r was defined for each mosaic as the value of average nearest distance between OFF cells). After the above calculation, the map was linearly rescaled to match the minimum and maximum value of the original SI values.

5.3. Relationship between ON-OFF RGC afferent distance and F_1/F_0 of V1 neuron

Based on previous studies (Mechler & Ringach, 2002; Priebe et al., 2004), the membrane voltage response of a V1 neuron to the drifting grating stimulus was modeled with a sinusoidal function:

$$V(t) = V_0 + V_1 cos(2\pi ft + \phi)$$

where V_0 represents the mean elevation of the membrane voltage and V_1 represents the amplitude of the modulation, f is the temporal frequency of the drifting grating, and ϕ is a constant phase term. The relationship between the membrane voltage fluctuation and F_1/F_0 was formulated using the following 3-parameter model:

$$F(V) = g[(V - V_{th})]_+^p$$

where F is spike rate, p is an exponent and g is a gain factor. For the simplest case, $p = 1$, the analytic expression of F_1/F_0 as a function of a variable $\chi = (V_{th} - V_0)/V_1$ can be obtained as follows (Mechler & Ringach, 2002).

$$\frac{F_1}{F_0} = \frac{-\chi\sqrt{1-\chi^2} + arccos(\chi)}{\sqrt{1-\chi^2} - \chi arccos(\chi)} \quad when\ -1 \le \chi \le 1$$
$$\frac{F_1}{F_0} = \frac{1}{\chi} \quad when\ \chi < -1 \tag{1}$$

From this, an analytically tractable model that expresses F_1/F_0 as a function of the distance between ON and OFF RGC afferents was formulated (Fig. 2f). A previous electrophysiological study showed that the response measured by firing of retinal ganglion cells varies sinusoidally with the matched temporal frequency of the drifting grating stimulus with optimal spatial frequency (Enroth-Cugell & Robson, 1966). Thus, a firing rate of an RGC to the drifting grating stimulus was described as a sinusoidal function, which is denoted as r(t).

$$r(t) = r_0 + r_1 cos(2\pi ft + \phi), \quad (r_0 > r_1\ for\ r(t) > 0)$$

where f is the temporal frequency of the drifting grating stimulus and ϕ is the phase determined by the location of the RGC receptive field (x). Note that for a suitable choice of reference, one can write the phase as a variable of spatial position divided by the spatial frequency (λ) of the drifting grating.

$$\phi = 2\pi * x/\lambda$$

Here, the value of λ was determined to produce the maximum response for each RGC, where the RGC receptive field was modeled as in the previous section and the response was calculated with a conventional linear nonlinear model (Chichilnisky, 2001). Summation of the response of ON and OFF RGCs at different positions (and thus different phases) yields the equation for the summed response, $r_{sum}(t)$.

$$r_{sum}(t) = r_{on} + r_{off} = r_{0,on} + r_{1,on} cos(2\pi ft + \phi_{on}) + r_{0,off} + r_{1,off} cos(2\pi ft + \pi + \phi_{off})$$

The addition of π phase arises from the opposite polarity of ON/OFF response. By letting $r_{0,on} = r_{0,off} = r_0, r_{1,on} = r_{1,off} = r_1$, and applying the trigonometric identity yields the simplified expression of the summed response.

$$r_{sum}(t) = 2r_0 + 2r_1 cos\left(\frac{\phi_{on}}{2} - \frac{\phi_{off}}{2} - \frac{\pi}{2}\right) \times cos\left(2\pi ft + \frac{\phi_{on}}{2} + \frac{\phi_{off}}{2} + \frac{\pi}{2}\right)$$

The interpretation of the above equation is as follows. The first term, $2r_0$, is independent of the phase difference between ON and OFF RGCs. The amplitude of the second term, however, is dependent on the phase difference between ON and OFF RGCs ($\phi_{on} - \phi_{off}$). When $\phi_{on} = \phi_{off}$, namely when ON and OFF receptive fields are completely overlapped, the amplitude of sinusoidal modulation becomes zero due to the $cos(0 + \frac{\pi}{2})$ term. As $\phi_{on} - \phi_{off}$ increases, the amplitude of sinusoidal modulation increases and becomes maximum when $\phi_{on} - \phi_{off} = \pi$.

Next, the expression of the membrane voltage fluctuation suggested by Mechler and Ringach was linked with the above expression of $r_{sum}(t)$ as follows.

$$V_0 \sim mean\,(r_{sum}(t)) = A * 2r_0$$

$$V_1 \sim |1st\ harmonic\ component\ of\ r_{sum}(t)|^k = B * \left(2r_1 cos\left(\frac{\phi_{on}}{2} - \frac{\phi_{off}}{2} - \frac{\pi}{2}\right)\right)^k$$

where the exponent k was applied for the expansive relationship between input and membrane voltage modulation that arises from nonlinear integration in dendrites (Polsky et al., 2004). This nonlinear relationship can generate a skewed distribution of V_1/V_0 as observed in cat (Priebe et al., 2004) from a Gaussian-like distribution of ON–OFF distance.

This sinusoidal membrane voltage fluctuation is rectified to generate spike response modulation. The expression that links the distance between ON/OFF afferent and χ, which determines the modulation ratio F_1/F_0 becomes,

$$\chi = \frac{V_{th} - V_0}{V_1} = \frac{V_{th} - 2Ar_0}{B\left(2r_1 cos\left(\phi_{on} - \phi_{off} - \frac{\pi}{2}\right)\right)^k} = c_1\left(cos\left(\phi_{on} - \phi_{off} - \frac{\pi}{2}\right)\right)^{-k} = c_1\left(cos\left(\frac{2\pi}{\lambda}(x_{ON} - x_{OFF}) - \frac{\pi}{2}\right)\right)^{-k}$$

where $c_1 = \frac{V_{th} - 2Ar_0}{B(2r_1)^k}$ is a constant. Substituting the χ into Eq. (1) and expressing the ON–OFF distance as $x_{ON} - x_{OFF} = d$, yields the analytic expression of F_1/F_0 in terms of d. Eq. (2) is given in Box I

From this expression, the distribution of F_1/F_0 can be calculated as in Fig. 2f of the main text. In our demonstration, $k = 3$, $c_1 \sim N$ (mean, std^2) $= N$ (-0.04, 0.08^2) were used (N represents the normal distribution).

5.4. Receptive field data

Receptive fields were analyzed using published data obtained by multielectrode recording in Layer 4 of cat V1, provided by Jose-Manuel Alonso via data presented in Fig. 2 of a previous study (Kremkow et al., 2016). The detailed experimental procedures for mapping receptive fields are described in the reference.

We defined the size of the receptive field (σ) for each recording site as the average radius of receptive fields within each penetration (assuming circular receptive fields). The distance between the center of mass of ON and OFF subfields was normalized by dividing that distance by r. The period of each distribution (SI, $d_{ON\text{-}OFF}$, and orientation preference) was calculated as the distance at which the pairwise difference value reaches its minimum among local minima of the curves, following the process to calculate the period of orientation preference in the reference (Kremkow et al., 2016).

5.5. Map simulation

The simulations were conducted based on the statistical wiring model published earlier (Paik & Ringach, 2011; Ringach, 2004, 2007). Here, we summarize the algorithm and parameters that were used to produce the results.

5.6. Generation of retinal ganglion cell mosaics

The ON and OFF RGC mosaics used in the simulation were generated by adding random spatial noise to each node of the hexagonal lattices that represent the position of the center of ON-center and OFF-center receptive fields, respectively. The position vectors of the centers of the receptive fields were defined as

$$\boldsymbol{x}_{ij,OFF} = d * \boldsymbol{H}_{ij} + \boldsymbol{\eta}_{ij}$$

$$\boldsymbol{x}_{ij,ON} = (1+\alpha)d * \boldsymbol{H}_{ij} + \boldsymbol{\eta}_{ij}$$

where d represents the lattice constant of the OFF mosaic, $(1 + \alpha)d$ represents the lattice constant of the ON mosaic ($\alpha = 1/7$), η_{ij} represents the 2-D additive Gaussian noise with a standard deviation $0.12d$ (so that a model mosaic has the similar nearest neighbor distance statistics as the measured mosaic Paik & Ringach, 2011), and $\boldsymbol{H}_{ij}$ represents the vectors of the nodes of a unit hexagonal lattice spanned by two basis vectors.

$$\boldsymbol{H}_{ij} = \frac{1}{2}\begin{bmatrix} 1 & 1 \\ \sqrt{3} & \sqrt{3} \end{bmatrix}\begin{bmatrix} i \\ j \end{bmatrix} \quad i, j \in \mathbb{Z}$$

The characteristic period of the hexagonal moiré interference pattern, λ_m, is given by (Blair et al., 2007)

$$\lambda_m = \frac{(1+\alpha)}{\alpha}d$$

when the directions of the two principal axes of the lattices match.

The main results of the model simulation and comparison with the data are nearly identical to the various choices of the parameter of the moiré interference.

5.7. Statistical connectivity and receptive field computation

The mean receptive field at each cortical site can be computed by the weighted sum of the afferent LGN input (it relays the afferent RGC input).

$$\Psi(x, y; \boldsymbol{x}) = \sum_i exp(-(\boldsymbol{x} - \boldsymbol{x_i})^2 / 2\sigma_{con}^2)\Psi_{i,LGN}$$

where $\boldsymbol{x}$ is the cortical site at which we calculate the mean receptive field, $\boldsymbol{x}_i$ is the location of the *ith* LGN afferent, $\psi_{i,LGN}$ is the receptive field of the LGN afferent, and σ_{con} ($= 0.325d$) is the parameter that determines the spatial extent of the synaptic weight distribution, which is assumed to be a form of Gaussian (Ringach, 2007; Sailamul et al., 2017). Previous work suggested that approximately six geniculate receptive fields are sufficient to match the size of a simple cell receptive field (Alonso et al., 2001). Based on this observation, along with the notion that the structure of each LGN receptive field is similar to that of a single RGC in most cases (Usrey et al., 1999), our model assumes that the retina-LGN-V1 feedforward connectivity is fairly well localized, with nearby V1 neurons tending to share a large portion

$$\frac{F_1}{F_0} = \frac{F_1}{F_0}(d) = \frac{-c_1\left(\cos\left(\frac{2\pi}{\lambda}d - \frac{\pi}{2}\right)\right)^{-k}\sqrt{1 - c_1^2\left(\cos\left(\frac{2\pi}{\lambda}d - \frac{\pi}{2}\right)\right)^{-2k}} + arccos\left(-c_1\left(\cos\left(\frac{2\pi}{\lambda}d - \frac{\pi}{2}\right)\right)^{-k}\right)}{\sqrt{1 - c_1^2\left(\cos\left(\frac{2\pi}{\lambda}d - \frac{\pi}{2}\right)\right)^{-2k}} + c_1\left(\cos\left(\frac{2\pi}{\lambda}d - \frac{\pi}{2}\right)\right)^{-k} arccos\left(-c_1\left(\cos\left(\frac{2\pi}{\lambda}d - \frac{\pi}{2}\right)\right)^{-k}\right)} \quad (2)$$
$$= \begin{cases} when\ -1 \le \chi \le 1, \\ \dfrac{1}{-c_1\left(\cos\left(\frac{2\pi}{\lambda}d - \frac{\pi}{2}\right)\right)^{-k}}\ when\ \chi < -1 \end{cases}$$

Box I.

of the local retinal feedforward projections. To implement this condition, approximately three to six RGCs are sampled with the Gaussian sampling range of $\sigma = 0.225$–0.325. Under this parameter condition, the preferred orientations of the local map appear consistent; thus, the periodic organization of the preferred orientation, $d_{ON\text{-}OFF}$, and SI are also fairly consistent (Supplementary Figure 2).

5.8. Measurements of cortical maps

Simulated cortical maps were obtained from the computed receptive fields at each cortical position. The SI of the V1 neurons was calculated in the same way as the SI of the data. The preferred orientation of each receptive field was calculated as the angle orthogonal to the line connecting the center of ON and OFF subregions. If either an ON or OFF subregion dominated (so called "monocontrast" cells, which respond to only one particular sign of contrast), so that the sum of all the weights of ON afferents was larger than two times the sum of all the weights of OFF afferents and vice versa, the neurons were excluded from the map measurement. After obtaining the SI and orientation preference of each cortical site, we smoothened the map with a 2-D Gaussian kernel with standard deviation $0.16\lambda_m$. The filtered map of SI and $d_{ON\text{-}OFF}$ was linearly rescaled to recover the minimum and maximum values of the raw cortical maps.

We obtained pixel-values from cross-sections of each simulated map along line segments that had the same length as the data segments, but with random penetration direction. The length of the data and model was normalized to match the period of orientation preference of the data (1.1 mm) and that of model (λ_m). As in the data, 27 sites with equal spacing were sampled for each cross-section (10,000 cross-sections) and pairwise difference curves were calculated. Two pairwise difference curves were randomly sampled and the mean and standard deviation of the mean of the two curves were calculated for 100,000 iterations.

The structural similarity among different maps was assessed at randomly sampled cortical lines (N = 10,000) by transforming orientation preference (θ) into $\cos(2\theta + \Phi)$ and spatially shifting to find the maximum correlation between preferred orientation and SI (or $d_{ON\text{-}OFF}$). The values of Φ (0–360°) and spatial shift (−0.5–0.5 mm) that maximize the correlation between $\cos(2\theta + \Phi)$ and SI along each penetration were determined iteratively. In the position-shuffled control dataset, the position information of each SI (or $d_{ON\text{-}OFF}$) value was randomly permuted.

CRediT authorship contribution statement

Gwangsu Kim: Designed the model, Performed the simulations, Analyzed the data, Drafted the manuscript, Discussed and commented on the manuscript. **Jaeson Jang:** Analyzed the data, Drafted the manuscript, Discussed and commented on the manuscript. **Se-Bum Paik:** Conceived the project, Designed the model, Analyzed the data, Wrote the final version of the manuscript with input from all authors, Discussed and commented on the manuscript.

Declaration of competing interest

The authors declare that they have no known competing financial interests or personal relationships that could have appeared to influence the work reported in this paper.

Data availability

All relevant data are available from the corresponding author upon request. The code used in this study is available at http://github.com/vsnnlab/SC.

Acknowledgments

We are grateful to Jose-Manuel Alonso (State University of New York) for sharing receptive field data on the cat primary visual cortex, via data presented in Fig. 2 of his reference (Kremkow et al., 2016). This work was supported by a National Research Foundation of Korea (NRF) grant funded by the Korean government (MSIT) (No. NRF-2019R1A2C4069863, NRF-2019M3E5D2A-01058328) (to S.P.).

Appendix A. Supplementary data

Supplementary material related to this article can be found online at https://doi.org/10.1016/j.neunet.2021.06.002. Supplementary material includes Supplementary Figures 1–6 and Supplementary Text.

References

Adelson, E. H., & Bergen, J. R. (1985). Spatiotemporal energy models for the perception of motion. *Journal of the Optical Society of America A*, *2*(2), 284.

Albus, K., & Wolf, W. (1984). Early post-natal development of neuronal function in the kitten's visual cortex: a laminar analysis. *The Journal of Physiology*, *348*(1), 153–185.

Almasi, A., Meffin, H., Cloherty, S. L., Wong, Y., Yunzab, M., & Ibbotson, M. R. (2020). Mechanisms of feature selectivity and invariance in primary visual cortex. *Cerebral Cortex (New York, N.Y.: 1991)*, *30*(9), 5067–5087.

Alonso, J.-M., & Martinez, L. M. (1998). Functional connectivity between simple cells and complex cells in cat striate cortex. *Nature Neuroscience*, *1*(5), 395–403.

Alonso, J.-M., Usrey, W. M., & Reid, R. C. (2001). Rules of connectivity between geniculate cells and simple cells in cat primary visual cortex. *The Journal of Neuroscience*, *21*(11), 4002–4015.

Antolik, J., & Bednar, J. A. (2011). Development of maps of simple and complex cells in the primary visual cortex. *Frontiers in Computational Neuroscience*, *5*.

Berkes, P., & Wiskott, L. (2005). Slow feature analysis yields a rich repertoire of complex cell properties. *Journal of Vision*, *5*(6), 579–602.

Blair, H. T., Welday, A. C., & Zhang, K. (2007). Scale-invariant memory representations emerge from moire interference between grid fields that produce theta oscillations: A computational model. *Journal of Neuroscience*, *27*(12), 3211–3229.

Braastad, B. O., & Heggelund, P. (1985). Development of spatial receptive-field organization and orientation selectivity in kitten striate cortex. *Journal of Neurophysiology*, *53*(5), 1158–1178.

Carandini, M., & Ferster, D. (2000). Membrane potential and firing rate in cat primary visual cortex. *Journal of Neuroscience*, *20*(1), 470–484.

Chance, F. S., Nelson, S. B., & Abbott, L. F. (1999). Complex cells as cortically amplified simple cells. *Nature Neuroscience*, *2*(3), 277–282.

Chichilnisky, E. J. (2001). A simple white noise analysis of neuronal light responses. *Network-Computation in Neural Systems*, *12*, 199–213.

Crair, M. C., Gillespie, D. C., & Stryker, M. P. (1998). The role of visual experience in the development of columns in cat visual cortex. *Science*, *279*(5350), 566–570.

Crowder, N. A., van Kleef, J., Dreher, B., & Ibbotson, M. R. (2007). Complex cells increase their phase sensitivity at low contrasts and following adaptation. *Journal of Neurophysiology*, *98*(3), 1155–1166.

De Valois, R. L., Albrecht, D. G., & Thorell, L. G. (1982). Spatial frequency selectivity of cells in macaque visual cortex. *Vision Research*, *22*(5), 545–559.

Dean, A. F., & Tolhurst, D. J. (1983). On the distinctness of simple and complex cells in the visual cortex of the cat. *The Journal of Physiology*, *344*(1), 305–325.

DeAngelis, G. C., Freeman, R. D., & Ohzawa, I. (1994). Length and width tuning of neurons in the cat's primary visual cortex. *Journal of Neurophysiology*, *71*(1), 347–374.

DeAngelis, G. C., Ohzawa, I., & Freeman, R. D. (1995). Receptive-field dynamics in the central visual pathways. *Trends in Neurosciences*, *18*(10), 451–458.

Enroth-Cugell, C., & Robson, J. G. (1966). The contrast sensitivity of retinal ganglion cells of the cat. *The Journal of Physiology*, *187*(3), 517–552.

Ferster, D., & Lindström, S. (1983). An intracellular analysis of geniculo-cortical connectivity in area 17 of the cat. *The Journal of Physiology*, *342*(1), 181–215.

Fournier, J., Monier, C., Pananceau, M., & Frégnac, Y. (2011). Adaptation of the simple or complex nature of V1 receptive fields to visual statistics. *Nature Neuroscience*, *14*(8), 1053–1060.

Gauthier, J. L., Field, G. D., Sher, A., Greschner, M., Shlens, J., Litke, A. M., & Chichilnisky, E. J. (2009). Receptive fields in primate retina are coordinated to sample visual space more uniformly. *PLoS Biology*, *7*(4), Article e1000063.

Ghosh, A., & Shatz, C. (1992). Pathfinding and target selection by developing geniculocortical axons. *The Journal of Neuroscience*, *12*(1), 39–55.

Hirsch, J. a., Gallagher, C. a., Alonso, J.-M., & Martinez, L. M. (1998). Ascending projections of simple and complex cells in layer 6 of the cat striate cortex. *The Journal of Neuroscience*, *18*(19), 8086–8094.

Hubel, D. H., & Wiesel, T. N. (1962). Receptive fields, binocular interaction and functional architecture in the cat's visual cortex. *The Journal of Physiology*, *160*(1), 106–154.

Jang, J., & Paik, S.-B. (2017). Interlayer repulsion of retinal ganglion cell mosaics regulates spatial organization of functional maps in the visual cortex. *The Journal of Neuroscience*, *37*(50), 12141–12152.

Jang, J., Song, M., & Paik, S.-B. (2020). Retino-cortical mapping ratio predicts columnar and salt-and-pepper organization in mammalian visual cortex. *Cell Reports*, *30*(10), 3270–3279.e3.

Jin, J., Wang, Y., Swadlow, H. A., & Alonso, J.-M. (2011). Population receptive fields of ON and OFF thalamic inputs to an orientation column in visual cortex. *Nature Neuroscience*, *14*(2), 232–238.

Kremkow, J., Jin, J., Wang, Y., & Alonso, J.-M. (2016). Principles underlying sensory map topography in primary visual cortex. *Nature*, *533*(7601), 52–57.

Lee, K.-S., Huang, X., & Fitzpatrick, D. (2016). Topology of ON and OFF inputs in visual cortex enables an invariant columnar architecture. *Nature*, *533*(7601), 90–94.

Lee, S.-H., Kwan, A. C., Zhang, S., Phoumthipphavong, V., Flannery, J. G., Masmanidis, S. C., Taniguchi, H., Huang, Z. J., Zhang, F., Boyden, E. S., Deisseroth, K., & Dan, Y. (2012). Activation of specific interneurons improves V1 feature selectivity and visual perception. *Nature*, *488*(7411), 379–383.

Lehky, S. R., Sejnowski, T. J., & Desimone, R. (2005). Selectivity and sparseness in the responses of striate complex cells. *Vision Research*, *45*(1), 57–73.

Li, Y., Ibrahim, L. A., Liu, B., Zhang, L. I., & Tao, H. W. (2013). Linear transformation of thalamocortical input by intracortical excitation. *Nature Neuroscience*, *16*(9), 1324–1330.

Lien, A. D., & Scanziani, M. (2013). Tuned thalamic excitation is amplified by visual cortical circuits. *Nature Neuroscience*, *16*(9), 1315–1323.

Lien, A. D., & Scanziani, M. (2018). Cortical direction selectivity emerges at convergence of thalamic synapses. *Nature*, *558*(7708), 80–86.

Litvina, E. Y., & Chen, C. (2017). Functional convergence at the retinogeniculate synapse. *Neuron*, *96*(2), 330–338.e5.

Mariño, J., Schummers, J., Lyon, D. C., Schwabe, L., Beck, O., Wiesing, P., Obermayer, K., & Sur, M. (2005). Invariant computations in local cortical networks with balanced excitation and inhibition. *Nature Neuroscience*, *8*(2), 194–201.

Martinez, L. M., & Alonso, J.-M. (2003). Complex receptive fields in primary visual cortex. *The Neuroscientist*, *9*(5), 317–331.

Martinez, L. M., Alonso, J.-M., Reid, R. C., & Hirsch, J. A. (2002). Laminar processing of stimulus orientation in cat visual cortex. *The Journal of Physiology*, *540*(1), 321–333.

Martinez, L. M., Wang, Q., Reid, R. C., Pillai, C., Alonso, J.-M., Sommer, F. T., & Hirsch, J. A. (2005). Receptive field structure varies with layer in the primary visual cortex. *Nature Neuroscience*, *8*(3), 372–379.

Mata, M. L., & Ringach, D. L. (2005). Spatial overlap of ON and OFF subregions and its relation to response modulation ratio in macaque primary visual cortex. *Journal of Neurophysiology*, *93*(2), 919–928.

Mechler, F., & Ringach, D. L. (2002). On the classification of simple and complex cells. *Vision Research*, *42*(8), 1017–1033.

Mooser, F., Bosking, W. H., & Fitzpatrick, D. (2004). A morphological basis for orientation tuning in primary visual cortex. *Nature Neuroscience*, *7*(8), 872–879.

Nauhaus, I., Nielsen, K. J., & Callaway, E. M. (2016). Efficient receptive field tiling in primate V1. *Neuron*, *91*(4), 893–904.

Nowak, L. G., Sanchez-Vives, M. V., & McCormick, D. A. (2010). Spatial and temporal features of synaptic to discharge receptive field transformation in cat area 17. *Journal of Neurophysiology*, *103*(2), 677–697.

Paik, S.-B., & Ringach, D. L. (2011). Retinal origin of orientation maps in visual cortex. *Nature Neuroscience*, *14*(7), 919–925.

Paik, S.-B., & Ringach, D. L. (2012). Link between orientation and retinotopic maps in primary visual cortex. *Proceedings of the National Academy of Sciences*, *109*(18), 7091–7096.

Polsky, A., Mel, B. W., & Schiller, J. (2004). Computational subunits in thin dendrites of pyramidal cells. *Nature Neuroscience*, *7*(6), 621–627.

Priebe, N. J., Mechler, F., Carandini, M., & Ferster, D. (2004). The contribution of spike threshold to the dichotomy of cortical simple and complex cells. *Nature Neuroscience*, *7*(10), 1113–1122.

Rao, S. C., Toth, L. J., & Sur, M. (1997). Optically imaged maps of orientation preference in primary visual cortex of cats and ferrets. *The Journal of Comparative Neurology*, *387*(3), 358–370.

Reid, R. C., & Alonso, J.-M. (1995). Specificity of monosynaptic connections from thalamus to visual cortex. *Nature*, *378*(6554), 281–284.

Ringach, D. L. (2002). Spatial structure and symmetry of simple-cell receptive fields in macaque primary visual cortex. *Journal of Neurophysiology*, *88*(1), 455–463.

Ringach, D. L. (2004). Haphazard wiring of simple receptive fields and orientation columns in visual cortex. *Journal of Neurophysiology*, *92*(1), 468–476.

Ringach, D. L. (2007). On the origin of the functional architecture of the cortex. *PLoS ONE*, *2*(2), Article e251.

Ringach, D. L., Shapley, R. M., & Hawken, M. J. (2002). Orientation selectivity in macaque V1: Diversity and laminar dependence. *The Journal of Neuroscience*, *22*(13), 5639–5651.

Rust, N. C., Schwartz, O., Movshon, J. A., & Simoncelli, E. P. (2005). Spatiotemporal elements of macaque V1 receptive fields. *Neuron*, *46*(6), 945–956.

Sailamul, P., Jang, J., & Paik, S.-B. (2017). Synaptic convergence regulates synchronization-dependent spike transfer in feedforward neural networks. *Journal of Computational Neuroscience*, *43*(3), 189–202.

Schein, S., & de Monasterio, F. (1987). Mapping of retinal and geniculate neurons onto striate cortex of macaque. *The Journal of Neuroscience*, *7*(4), 996–1009.

Seriès, P., Lorenceau, J., & Frégnac, Y. (2003). The silent surround of V1 receptive fields: theory and experiments. *Journal de Physiologie (Paris)*, *97*(4–6), 453–474.

Sharpee, T., Rust, N. C., & Bialek, W. (2004). Analyzing neural responses to natural signals: Maximally informative dimensions. *Neural Computation*, *16*(2), 223–250.

Shatz, C., & Luskin, M. (1986). The relationship between the geniculocortical afferents and their cortical target cells during development of the cat's primary visual cortex. *The Journal of Neuroscience*, *6*(12), 3655–3668.

Skottun, B. C., De Valois, R. L., Grosof, D. H., Movshon, J. A., Albrecht, D. G., & Bonds, A. B. (1991). Classifying simple and complex cells on the basis of response modulation. *Vision Research*, *31*(7–8), 1079–1086.

Song, M., Jang, J., Kim, G., & Paik, S.-B. (2021). Projection of orthogonal tiling from the retina to the visual cortex. *Cell Reports*, *34*(1), Article 108581.

Soodak, R. E. (1987). The retinal ganglion cell mosaic defines orientation columns in striate cortex. *Proceedings of the National Academy of Sciences of the United States of America*, *84*(11), 3936–3940.

Swindale, N. V., Shoham, D., Grinvald, A., Bonhoeffer, T., & Hübener, M. (2000). Visual cortex maps are optimized for uniform coverage. *Nature Neuroscience*, *3*(8), 822–826.

Tao, L., Shelley, M., McLaughlin, D., & Shapley, R. (2004). An egalitarian network model for the emergence of simple and complex cells in visual cortex. *Proceedings of the National Academy of Sciences*, *101*(1), 366–371.

Touryan, J., Felsen, G., & Dan, Y. (2005). Spatial structure of complex cell receptive fields measured with natural images. *Neuron*, *45*(5), 781–791.

Usrey, W. M., Reppas, J. B., & Reid, R. C. (1999). Specificity and strength of retinogeniculate connections. *Journal of Neurophysiology*, *82*(6), 3527–3540.

Van Hooser, S. D., Roy, A., Rhodes, H. J., Culp, J. H., & Fitzpatrick, D. (2013). Transformation of receptive field properties from lateral geniculate nucleus to superficial V1 in the tree shrew. *Journal of Neuroscience*, *33*(28), 11494–11505.

Vidne, M., Ahmadian, Y., Shlens, J., Pillow, J. W., Kulkarni, J., Litke, A. M., Chichilnisky, E. J., Simoncelli, E., & Paninski, L. (2012). Modeling the impact of common noise inputs on the network activity of retinal ganglion cells. *Journal of Computational Neuroscience*, *33*(1), 97–121.

Wassle, H., Boycott, B. B., & Illing, R. B. (1981). Morphology and mosaic of on- and off-beta cells in the cat retina and some functional considerations. *Proceedings of the Royal Society of London. Series B. Biological Sciences*, *212*(1187), 177–195.

Wiskott, L., & Sejnowski, T. J. (2002). Slow feature analysis: Unsupervised learning of invariances. *Neural Computation*, *14*(4), 715–770.

Yu, J., & Ferster, D. (2013). Functional coupling from simple to complex cells in the visually driven cortical circuit. *Journal of Neuroscience*, *33*(48), 18855–18866.

Zhan, X. J., & Troy, J. B. (2000). Modeling cat retinal beta-cell arrays. *Visual Neuroscience*, *17*(1), 23–39.